Direct Photocatalytic Synthesis of Acetic Acid from Methane and CO at Ambient Temperature using Water as Oxidant

Chunyang Dong,[1] Maya Marinova,[2] Karima Ben Tayeb,[3] Olga V. Safonova,[4] Yong Zhou,[1] Di Hu,[1] Sergei Chernyak,[1] Massimo Corda,[1] Jérémie Zaffran,[1] Andrei Y. Khodakov[1*] and Vitaly V. Ordomsky[1*]

1. UCCS–Unité de Catalyse et Chimie du Solide, Université de Lille, CNRS, Centrale Lille, ENSCL, Université d'Artois, UMR 8181, F-59000 Lille, France.
2. UMET–Institut Michel-Eugène Chevreul, Université de Lille, CNRS, INRAE, Centrale Lille, Université d'Artois, FR 2638, F-59000 Lille, France.
3. Université de Lille, CNRS, UMR 8516 - LASIRE - Laboratoire de Spectroscopie pour les Interactions, la Réactivité et l'Environnement, F-59000 Lille, France.
4. Paul Scherrer Institute, 5232 Villigen, Switzerland.

Corresponding authors: Andrei Y. Khodakov (Andrei.Khodakov@univ-lille.fr); Vitaly V. Ordomsky (Vitaly.Ordomsky@univ-lille.fr)

Abstract

Direct functionalization of methane selectively to value-added chemicals is still one of the main challenges in modern science. Acetic acid is an important industrial chemical produced nowadays by expensive and environmentally unfriendly carbonylation of methanol using homogeneous catalysts. Here, we report a new photocatalytic reaction route to synthesize acetic acid from CH_4 and CO at room temperature using water as the sole external oxygen source. The optimized photocatalyst consists of TiO_2 support and ammonium phosphotungstic polyoxometalate (NPW) clusters anchored with isolated Pt single atoms (Pt_1). It enables a stable synthesis of 5.7 mmol·L^{-1} acetic acid solution in 60 hours with the selectivity over 90 and 66% to acetic acid on liquid-phase and carbon basis, respectively, with the production of 99 mol of acetic acid per mol of Pt. Combined isotopic and *in-situ* spectroscopy investigation suggests that synthesis of acetic acid proceeds via a photocatalytic oxidative carbonylation of methane over the Pt_1 sites, with the methane activation facilitated by water-derived hydroxyl radicals.

Introduction

Methane is one of the most abundant carbonaceous reserve feedstocks and also a notorious greenhouse gas. Its catalytic conversion towards value-added liquid oxygenates attracts considerable interest from the scientific community.[1-3] The current industrial route for methane transformation to obtain acetic acid (AcOH) is an energy-intensive and indirect multistep route through methane reforming to syngas (CO and H_2), methanol synthesis and subsequent methanol carbonylation to AcOH.[4-5] Direct routes of methane transformation to AcOH under mild conditions also have been explored in the literature, such as the Pd(II) catalyzed oxidative methane condensation in liquid sulfuric acid,[6-7] Ca- and V-complex catalyzed methane carboxylation with peroxodisulfate and trifluoroacetic acid,[8-9] methane carbonylation with CO and O_2, catalyzed by homo- and heterogeneous Rh single sites, etc.[10-13] However, the indispensable use of strong oxidants such as corrosive acid or molecular oxygen inevitably leads to environmental issues, safety risks, and low selectivity due to the overoxidation of AcOH to carbon oxides. Consequently, realizing mild selective oxidation of methane to concentrated AcOH, while avoiding the use of aggressive chemicals, would be highly desirable.

Environmentally friendly and abundant water is a widely used solvent and oxygen source in many fundamental catalytic reactions.[14-16] Previously, Sushkevich et al. showed that water could act as both a soft oxidant and an intermediate stabilizer in the anaerobic oxidation of methane and thus, contribute to high selectivity to methanol.[15] More recently, Liu et al. further elaborated on the promotion effect of water as both O-provider and site-blocker in the CH_4 oxidation to methanol.[16] The challenge of the direct AcOH synthesis from CH_4, CO and water, however, lies in the unfavorable thermodynamics (**eq. 1-2** and **Figure S1**).

$$CH_4 + CO + H_2O = CH_3COOH + H_2 \qquad (1)$$

$$2CH_4 + 2H_2O = CH_3COOH + 4H_2 \qquad (2)$$
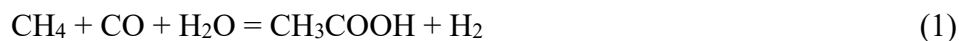
By utilizing photo-excited charge carriers as the driving force for the activation of chemical bonds, photocatalysis provides an opportunity to overpass the thermodynamic limitations of conventional thermo-activated catalysis.[17-21] Specifically, with suitable

photocatalytic systems, CH_4, CO and water could be activated even under room temperature (e.g., non-oxidative CH_4 coupling to C_2H_6, overall water splitting, etc.),[22-26] thus, making feasibile and sustainable the above H_2O-induced oxidative transformation of CH_4 into AcOH.

Herein, we report a direct photocatalytic synthesis of AcOH from methane and CO at ambient temperature over a ternary-phase composite constituted of TiO_2 and Pt_1 anchored ammonium phosphotungstic polyoxometalate (i.e., $(NH_4)_xPW_{12}O_{40}$, abbreviated as NPW) sub-nano clusters, using water as the sole external oxygen source. Under an optimized condition, our catalyst enables a stable synthesis of 5.7 mmol·L^{-1} AcOH solution with a liquid-phase selectivity of over 90% in 60 hours and a Turnover Number (TON) of about 99.

Results and Discussion

Direct photocatalytic synthesis of AcOH from CH_4, CO, and H_2O.

The photocatalysts, which we used for CH_4 transformation reactions are composites constituted by TiO_2 (commercial P25) and Pt-anchored NPW. The catalyst synthesis was realized by stepwise precipitating Pt-anchored NPW particles and mixing them with TiO_2 via grinding and heat treatment (see Methods section in Supporting Information for more details). The catalysts with other group VIII metals (Pd, Rh, Co, Ru) and SiO_2 instead of TiO_2 have been prepared in the same way. Unless otherwise specified, metal loading in different M/NPW is kept at 1 wt.% and the preliminary weight ratio between M/NPW and TiO_2 is set at 3:5.
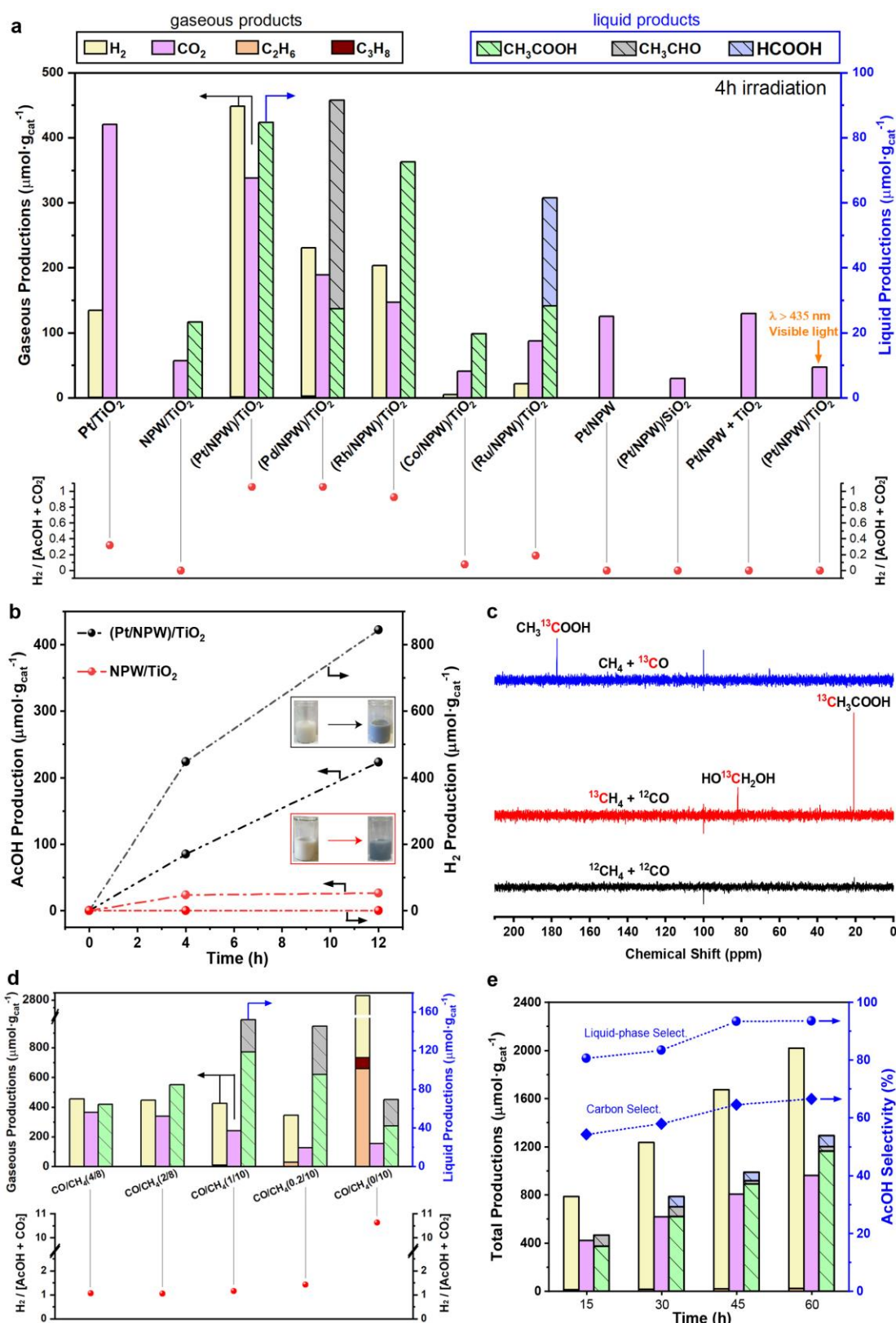
Figure 1. Photocatalytic evaluation of AcOH synthesis. (a) Activities and molar ratios between produced H_2 and [AcOH + CO_2] of different catalysts after 4 h irradiation. (b) Time course evolution of AcOH and H_2 over NPW/TiO_2 (3:5) and (Pt/NPW)/TiO_2 (3:5) in 12 h. The inset images are photos of the catalyst-water

suspension before and after 12 h irradiation. (c) ^{13}C-NMR spectra of liquid products of (Pt/NPW)/TiO$_2$ (3:5) with $^{12}CH_4 + ^{12}CO$, $^{13}CH_4 + ^{12}CO$, and $^{12}CH_4 + ^{13}CO$. (d) Catalytic performance and molar ratios between produced H$_2$ and [AcOH + CO$_2$] of (Pt/NPW)/TiO$_2$ (3:5) after 4 h irradiation at different CO/CH$_4$ bars. (e) The total accumulated products and the liquid-phase selectivity of AcOH of (Pt/NPW)/TiO$_2$ (3:10) under 1 bar CO and 10 bar CH$_4$. General reaction conditions: 50 mg catalyst, 10 mL H$_2$O, 20 $^{\circ}$C, and a 400 W Hg-Xe lamp as the light source.

The photocatalytic CH$_4$ conversion was performed in a 100 mL batch photoreactor, with a 400 W Hg-Xe lamp used as a light source. Throughout the reaction, the catalyst-water suspension (10 mL) was magnetically stirred, and the reaction temperature was kept at 20 $^{\circ}$C. First, the productivities of different catalysts after 4 h light irradiation under 2 bar CO and 8 bar CH$_4$ are summarized in **Figure 1a**. Pt/TiO$_2$ can only transform CO and/or CH$_4$ to CO$_2$ and H$_2$ without the generation of valuable liquid oxygenates. The nonstoichiometric ratio between CO$_2$ and H$_2$, which should be equal to one in the case of water-gas shift (WGS) reaction, indicates that a part of oxygen species for CO and/or methane oxidation to CO$_2$ comes from the catalysts (see **Figure S2** and related discussion in SI).[27] As for Pt/NPW, (Pt/NPW)/SiO$_2$ and freshly mixed Pt/NPW + TiO$_2$ (i.e., without grinding and heat treatment), CO$_2$ is the only detectable product. The production of AcOH was observed only for (M/NPW)/TiO$_2$ (M = Pt, Pd, Rh, Co and Ru) and NPW/TiO$_2$ that underwent grinding and heat treatment procedures. Remarkably, (Pt/NPW)/TiO$_2$ shows the highest activity among others, with an AcOH production of 84.7 μmol$\cdot$g$_{cat}^{-1}$ after 4 h irradiation. No oxygen was detected during the CH$_4$ photocatalytic conversion.

When (Pt/NPW)/TiO$_2$ was irradiated with visible light ($\lambda > 435$ nm), only a very tiny amount of CO$_2$ was produced (**Figure 1a**). Together with the similar catalytic behavior of Pt/NPW and (Pt/NPW)/SiO$_2$ under full irradiation, these results suggest that the AcOH synthesis over (Pt/NPW)/TiO$_2$ is essentially driven by photo-induced charge carriers from TiO$_2$ (see **Figure S3** and related discussion in SI).

Eqs. (1) and (2) suggest a stable steady-state production of AcOH either from water-induced oxidative CH$_4$ condensation or from CH$_4$ carbonylation by CO. The latter

should be accompanied by the evolution of the equivalent amount of H_2 to the amount of produced AcOH. Together with the competitive WGS reaction, the total amount of CO_2 and AcOH in each batch should be approximately equal to the production of H_2. Interestingly, only (Pt/NPW)/TiO_2, (Pd/NPW)/TiO_2 and (Rh/NPW)/TiO_2 manifested an equivalent production of H_2 and [CO_2 + AcOH] (**Figure 1a**). Somewhat lower hydrogen production for other catalysts can be attributed to the partial reduction of NPW and metal oxide species with H_2, which do not contain Pt, Pd and Rh.

Consequently, in contrast to the stable AcOH production over (Pt/NPW)/TiO_2 (**Figure 1b**), for NPW/TiO_2, the production of AcOH was observed only during the initial period. After 12 h irradiation, both two catalysts changed their color to dark blue (inset images in **Figure 1b**). The blue color should be attributed to the formation of partially reduced NPW (i.e., heteropoly blue).[28] This suggests that methane oxidation over both NPW/TiO_2 and (Pt/NPW)/TiO_2 might involve NPW lattice oxygen[29]:

$$CH_4 + CO + NPW = CH_3COOH + NPW[Ov] \tag{3}$$

The depletion of these oxygen species may cause the deactivation of NPW/TiO_2. Interestingly, exposing the deactivated NPW/TiO_2 to air for 2h under stirring can restore both its color and reactivity for the next cycle (**Figure S4**). The observed stability of (Pt/NPW)/TiO_2 indicates that Pt species are capable of utilizing H_2O as the external oxidant for regeneration of NPW oxygen species and simultaneously produce H_2.

Furthermore, we studied the influence of CO/CH_4 ratios on the catalytic performance of (Pt/NPW)/TiO_2. As shown in **Figure 1d**, after 4 h irradiation, the highest production of AcOH of 118.5 $\mu mol \cdot g_{cat}^{-1}$ was achieved at 1 bar CO and 10 bar CH_4. The high productivity is accompanied by additional acetaldehyde production with a liquid-phase selectivity to AcOH of 78 %. Acetaldehyde could derive from the intermediates of AcOH synthesis. Under light irradiation, the transformation of acetaldehyde and H_2O into AcOH and H_2 is quite facile over (Pt/NPW)/TiO_2 (see **Figure S5** and related discussion in SI). Notably, decreasing the CO partial pressure from 4 bar to 0.2 bar can drastically reduce the production of CO_2 from 363.6 to 126.7 $\mu mol \cdot g_{cat}^{-1}$, while the total amount of CO_2 and AcOH are approximately equal to the productions of H_2 under the mixed CO/CH_4 atmospheres for the (Pt/NPW)/TiO_2, (Pd/NPW)/TiO_2 and

(Rh/NPW)/TiO$_2$ catalysts (**Figure 1d**). Besides, under the atmosphere of 4 bar CO (without CH$_4$), nearly equal amounts of CO$_2$ and H$_2$ were observed at different reaction times (**Figure S6**). In this case, both CO$_2$ and H$_2$ were produced by the water gas shift reaction. No AcOH or acetaldehyde was observed. When the reaction was performed in 10 bar CH$_4$ at the CO/CH$_4$ ratio of 0/10, the production of significant amounts of C$_2$H$_6$, C$_3$H$_8$, and H$_2$ suggests that the non-oxidative methane coupling to ethane became the dominant reaction path, in the meanwhile, the production of AcOH decreased by a factor of 3 (**Figure 1d**). The small production of AcOH from methane in the absence of externally added CO may result from the coupling of methane and CO produced during methane partial oxidation. In the following catalytic tests, the irradiation time was extended to 15 h at optimal conditions, which correspond to 1 bar CO and 10 bar CH$_4$. These conditions enable the highest AcOH productivity.

The chemical composition of the (Pt/NPW)/TiO$_2$ catalysts was optimized by varying the contents of Pt/NPW and Pt. Eventually, the catalyst with 0.2 wt.% Pt loading and the weight ratio between Pt/NPW and TiO$_2$ at 3:10 exhibited the highest AcOH productivity (374.4 μmol·g$_{cat}^{-1}$) among others (**Figures S7-S9**). Under the 360 nm monochromatic light, a 2.55 % apparent quantum yield (AQY) was achieved (see **Methods section in Supporting Information** for more details). This AQY is comparable to the most advanced photocatalytic methane transformation systems in nonoxidative coupling (**Table S1**).[2-3, 20, 30-33] Note that this AQY in this work was achieved using water as a soft oxidizing agent and without the use of toxic or aggressive oxidants such as H$_2$O$_2$ or O$_2$.

Moreover, the optimized (Pt/NPW)/TiO$_2$ (3:10) catalyst demonstrated superior photochemical stability and selectivity (**Figure 1e**). In the absence of any regeneration treatment, under 1 bar CO and 10 bar CH$_4$, 1166 μmol·g$_{cat}^{-1}$ AcOH was produced after four reaction cycles for a total of 60 h irradiation. The production rate of AcOH was 24.9 μmol·h^{-1}g$_{cat}^{-1}$ in the first 15h, 16.5 μmol·h^{-1}g$_{cat}^{-1}$, between 15 and 30 h, 17.9 μmol·h^{-1}g$_{cat}^{-1}$ in the 30-45 h time period and 18.4 μmol·h^{-1}g$_{cat}^{-1}$ between 45 and 60 h. The decrease in the AcOH amount after the first cycle can be attributed to its slow decomposition (**Figure S10**). The reaction proceeded with a TON of 99 assuming that

the reaction involves Pt sites and yielded an aqueous AcOH solution with a concentration of 5.7 mmol·L^{-1}. Besides, over the whole cyclic test, the AcOH selectivity of the (Pt/NPW)/TiO$_2$ (3:10) remained around 80 – 90 % in the liquid-phase with only a small amount of acetaldehyde and formic acid as side products (**Figure S8**). Interestingly, CO adsorption over Pt sites during the reaction preserves the AcOH from rapid decomposition (see **Figure S10** and related discussion in SI). This suggests that CO can block the sites of acetic acid decomposition. Remarkably, compared to previous studies including both homogeneous and heterogeneous catalytic systems, our optimized (Pt/NPW)/TiO$_2$ (3:10) catalyst also demonstrates a higher liquid-phase selectivity towards AcOH in the long reaction process (**Table S2**).[6, 9-10, 12-13, 34-36] Importantly, different to previous reports, high AcOH productivities in the present work were achieved at ambient temperature. The details of the reaction mechanism of AcOH photocatalytic synthesis from methane, CO and water are discussed below in a dedicated section.
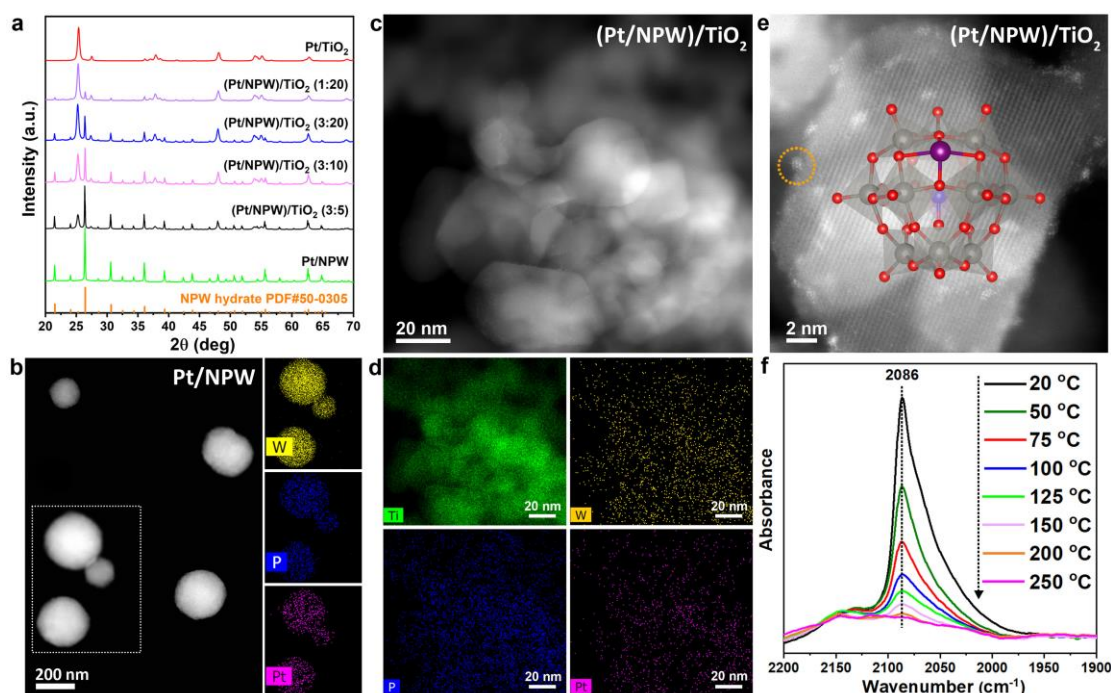
Figure 2. Structural characterizations of (Pt/NPW)/TiO$_2$ composites. (a) XRD patterns of different catalysts. HAADF-STEM and corresponding EDS-mapping images of Pt/NPW (b) and (Pt/NPW)/TiO$_2$ (3:10) (c-d). (e) Atomic-resolved HAADF-STEM image of Pt/NPW/TiO$_2$ (3:10), the inset image represents the monomer of Keggin-structured NPW with isolated Pt atoms anchored at 4-fold hollow site of W-O-

W, color code: red (oxygen), grey (tungsten), blue (phosphorus), purple (platinum). (f) IR spectra of temperature-programmed CO desorption over (Pt/NPW)/TiO$_2$ (3:10).

Besides selectivity, the conversion and product yield are highly important for industrial applications due to the high energy consumption for separation and recycling. The conversion of CH$_4$ in a 100 mL reactor after 60 h irradiation is around 0.15 %. By increasing the amount of catalyst to 250 mg and decreasing the gaseous volume of the reactor to 45 mL, the 0.33% CH$_4$ conversion was achieved after 15 h irradiation. Note that this yield of AcOH was achieved at ambient temperature using water as a soft oxidizing agent.

Catalyst characterization

In order to provide further insights into the catalytic active sites for AcOH production, we investigated the structure of (Pt/NPW)/TiO$_2$. The XRD patterns of Pt/NPW, Pt/TiO$_2$, and (Pt/NPW)/TiO$_2$ with different Pt/NPW contents are shown in **Figure 2a**. Pure Pt/NPW shows narrow diffraction peaks characteristic of the Keggin-type NPW (PDF#50-0305) crystalline phase. This indicates large crystallite sizes of Pt/NPW. The (Pt/NPW)/TiO$_2$ composites demonstrate the presence of both TiO$_2$ and Keggin-type NPW crystalline phases. With the decrease in the (Pt/NPW) content, the intensity of NPW signals decreases accordingly, until almost complete disappearance of NPW XRD peaks at the (Pt/NPW)/TiO$_2$ ratio of 1:20.

The space-resolved atomic-scale structures of the (Pt/NPW)/TiO$_2$ samples are probed by aberration-corrected scanning transmission electron microscopy (STEM). Without TiO$_2$, STEM images of Pt/NPW show large polyhedral particles with a diameter of several hundred nanometers (**Figure 2b**). The high-angle annular dark-field (HAADF) imaging cannot distinguish Pt from W due to the similar atomic weights. The energy-dispersive X-ray spectroscopy (EDS) mapping uncovered in the samples the Pt species homogeneously dispersed over individual NPW polyhedrons (**Figure 2b**). Surprisingly, grinding together Pt/NPW and TiO$_2$ followed by calcination gives rise to the formation of a sub-monolayer coating of polyoxometalate clusters over TiO$_2$ nanocrystals. Taking the optimal (Pt/NPW)/TiO$_2$ (3:10) composite as an example, STEM and corresponding

EDS-mapping images demonstrated highly dispersed W-, P- and Pt- species on TiO_2 (**Figure 2c-d**). The atomic-resolved HAADF imaging showed that these highly dispersed species were isolated Keggin-type NPW clusters (**Figure 2e**). A large-scale STEM imaging uncovered that undispersed Pt/NPW polyhedrons were localized around TiO_2 (**Figure S11**). The (Pt/NPW)/TiO_2 (1:20) catalyst with the lowest Pt/NPW content exhibited similar high dispersion of Pt/NPW. However, the surface coverage of TiO_2 with Pt/NPW was much lower (**Figure S12**). Characterization of (Pt/NPW)/TiO_2 (3:10) after 15 h photocatalytic reaction using STEM and corresponding EDS images showed stability of the fine atomic structure. This observation is consistent with the excellent (Pt/NPW)/TiO_2 photocatalytic stability (**Figure S13**).

According to previous studies, transition metals could be anchored by Keggin-type polyoxometalate in an atomically dispersed state, with one metal atom placed at the 4-fold hollow site, coordinated by 4 oxygen atoms of polyoxometalate.[37-39] To evaluate the Pt dispersion, the temperature-programmed desorption (TPD) of CO with the simultaneous characterization of surface species by IR was performed for (Pt/NPW)/TiO_2 (3:10). The catalyst has been pretreated *in-situ* in the atmosphere of CH_4 and CO (0.1 bar CO and 0.9 bar CH_4) under UV light irradiation. After 60 min irradiation, an intense absorption band centered at 2086 cm^{-1} was observed and assigned to the CO adsorption over Pt species (**Figure 2f**).[40-41] An increase in the temperature from 20 to 250 $^{\circ}C$ in the vacuum without irradiation resulted in the gradual desorption of CO from the catalyst. The band position of CO was kept consistently at 2086 cm^{-1} along with the reduction of CO coverage, indicating the absence of the dipole-dipole interaction between the adsorbed CO molecules and confirming atomic dispersion of primary Pt species over the catalyst.[42-43]

Thus, the characterization results are indicative of a high dispersion of Pt_1 anchored NPW polyhedrons over TiO_2. According to our previous study, the precipitated phosphotungstic polyoxometalates exhibit noticeable acidity.[2] Therefore, during the heat treatment process, it is believed that the acidity drives the Pt/NPW aggregates disassembling over the basic TiO_2 surface. Indeed, the dispersion of Pt/NPW aggregates is significantly higher over supports containing basic sites (e.g., TiO_2, Al_2O_3 and ZnO)

than more acid supports such as SiO_2 (**Figure S14-16**).[44-45] Since these sub-nanometric Pt/NPW clusters played a key role in the catalytic performance of AcOH synthesis (**Figure 1**), eventually, the catalyst with a lesser content of Pt/NPW exhibited even higher dispersion of Pt/NPW active phase and consequently higher Pt-normalized activity in the AcOH production (**Figure S7**).

Reaction mechanism of the catalytic synthesis of AcOH.

Generally, the light excitation of semiconductors, the spatial separation and transfer of photo-excited charge carriers and the surface catalytic reaction constituted the three key steps within a photocatalytic reaction. In the following section, we investigated the mechanism of photocatalytic synthesis of AcOH from methane, CO and water using a combination of *in-situ* spectroscopic and isotope methods.
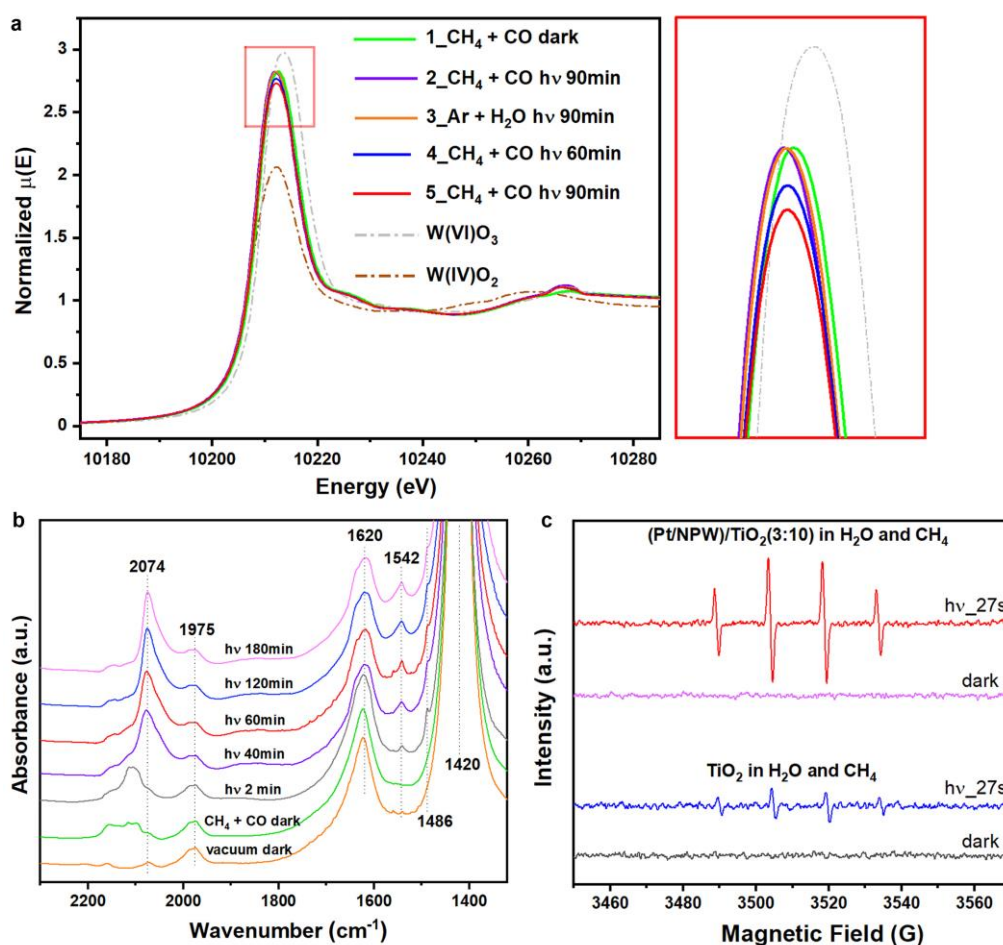
Figure 3. Mechanistic studies of AcOH synthesis. (a) *in-situ* W L_3-edge XANES spectra recorded during the interaction of (Pt/NPW)/TiO$_2$ (3:20) with different feed gas

flow under dark and light irradiation. (b) *In-situ* IR spectra recorded during the interaction between (Pt/NPW)/TiO$_2$ (3:5) and atmospheric CO/CH$_4$ mixture under dark and light irradiation conditions. (c) *In-situ* EPR spectra recorded at room temperature during the interaction of different catalysts with CH$_4$ under dark and light irradiation conditions in the presence of DMPO.

The in-situ X-ray absorption spectroscopy has provided detailed information about the variation of the oxidation state of tungsten during the photocatalytic reaction in the catalyst with a lower Pt/NPW content. In **Figure 3a**, the X-ray absorption near edge structure (XANES) spectra of W L$_3$-edge of (Pt/NPW)/TiO$_2$ (3:20) were recorded during the interaction with different gases (i.e., CH$_4$/CO or Ar/H$_2$O). The intensity of W L$_3$-edge white line (as a consequence of electron transition from 2p$_{3/2}$ state to vacant 5d state[46]) correlates to the oxidation state of tungsten.[47] Only marginal variations of the white line have been noticed upon light irradiation of the catalyst in both CH$_4$/CO and Ar/H$_2$O (spectra 2 and 3). A slight decrease in the intensity of the white line was observed after long exposure of the catalyst to CH$_4$/CO (spectra 4 and 5), which could be indicative of the gradual reduction of W species. This is consistent with the earlier observed color changes of (Pt/NPW)/TiO$_2$, which corresponds to the partial reduction of tungsten species in CH$_4$/CO. No AcOH and acetaldehyde productions were observed for both (Pt/NPW)/TiO$_2$ and (NPW)/TiO$_2$ without water (**Figure S17**).

To confirm the roles of CH$_4$ and CO in the AcOH synthesis process, we performed isotopic labelling tests with the ^{13}C-labelled reactants over (Pt/NPW)/TiO$_2$ (3:5). As shown in **Figure 1c**, when ^{13}CH$_4$ + CO or CH$_4$ + ^{13}CO are used as reactants, ^{13}C NMR spectra manifest respectively prominent signals at $\delta = 20.8$ and $\delta = 178$, which are ascribed to ^{13}CH$_3$COOH and CH$_3$^{13}COOH. This suggests that the methyl groups are derived from CH$_4$, while acyl groups of AcOH are produced from CO.

Only negligible ^{13}CO$_2$ production was observed when ^{13}CH$_4$ + ^{12}CO are used as reactants (**Figure S18**). This suggests that CO$_2$ is principally produced from CO by the photocatalytic water-gas shift reaction. The oxidation of CH$_4$ to CO$_2$ is, therefore, negligible under these conditions.

In-situ FTIR measurements were performed to understand the evolution of surface

intermediates under irradiation (**Figure 3b**). Under vacuum and in the dark, the fresh (Pt/NPW)/TiO$_2$ (3:5) composite manifests two intense absorption bands at 1420 and 1620 cm^{-1}, corresponding respectively to the vibration of NH$_4^+$ in NPW and adsorbed H$_2$O species.[37, 48] Introducing 0.1 bar CO and 0.9 bar CH$_4$ to the catalyst only brings the peak of adsorbed CO on the cationic Pt species between 2150 to 2100 cm^{-1}. Significantly, upon irradiation, except for the evolution of CO adsorption bands over reduced Pt$_1$ sites at 2074 cm^{-1}, newly formed bands centered at 1486 and 1542 cm^{-1}, are immediately observed. They are attributed to the symmetric (ν_s) and asymmetric (ν_{as}) vibration of bidentate acetate (*CH$_3$COO, the asterisk denotes as adsorbed states).[49-51] With the prolongation of irradiation time, the band of ν_{as}(*CH$_3$COO) became more and more intense, while the intensity of the peak at 1620 cm^{-1} gradually decreases. The decrease in the intensity of the band at 1620 cm^{-1} corresponds to the consumption of adsorbed H$_2$O by the photocatalytic reaction. This observation is consistent with the essential role of H$_2$O in the catalytic synthesis of AcOH from CH$_4$ and CO.

The solid-state electron paramagnetic resonance (EPR) spectra of TiO$_2$, and (Pt/NPW)/TiO$_2$ (3:10) that were recorded at 120 K are shown in **Figure S19.** They exhibit the signals attributed to lattice-trapped electrons in both anatase (g⊥=1.993) and rutile (g⊥=1.985) and surface-trapped holes.[52] The oxygen-centered radical, due to the trapping of holes on the surface of titania, is characterized by g$_x$ = 2.006, g$_y$ = 2.016, and g$_z$ = 2.030 and can be assigned to the (Ti^{4+}O$^{•-}$)$_{surf}$ paramagnetic species. The higher intensity of these signals in (Pt/NPW)/TiO$_2$ (3:10) compared to TiO$_2$ indicates enhanced charge carrier separation in the (Pt/NPW)/TiO$_2$ composite photocatalyst. According to a recent study by Streb et al., phosphotungstic polyoxometalate can act as electron storage sites during photocatalysis, accepting photo-excited electrons and releasing them in the absence of light.[53] In line with their study, higher intensity of lattice trapped electrons in the dark suggests an electron backflow from Pt/NPW to TiO$_2$. Together with the prominent color variation of the catalysts under light irradiation, it is indicated that the sub-nanometric Pt/NPW clusters promoted the charge separation efficiency of TiO$_2$ by accepting photo-excited electrons.

Subsequently, to gain more insight into the H$_2$O-induced oxidative methane

activation process, we performed *in-situ* EPR analysis under simulated reaction conditions. During the test, 5,5-dimethyl-1-pyrrolyne N-oxide (DMPO) was used as the radical trapping agent. Intensive signals of hydroxyl radical ($\cdot$OH) were immediately observed upon irradiation, while the signals of methyl radical ($\cdot CH_3$) were hardly noticed in both CH_4/CO mixture and the pure CH_4 atmosphere (**Figure 3c** and **Figure S20**). The absence of methyl radicals suggests that methyl group could be immediately consumed over Pt_1 sites during the reaction.[54] Scavenging of reactive oxygen species (ROS) using salicylic acid and sodium oxalate indicate that $\cdot$OH also played fundamental roles in promoting methane activation. In the absence of $\cdot$OH, the generation of AcOH and H_2 was ceased completely (**Figure S21**). Note that we did not detect hydrogen peroxide (H_2O_2) by iodine method during AcOH synthesis process (**Figure S22**).
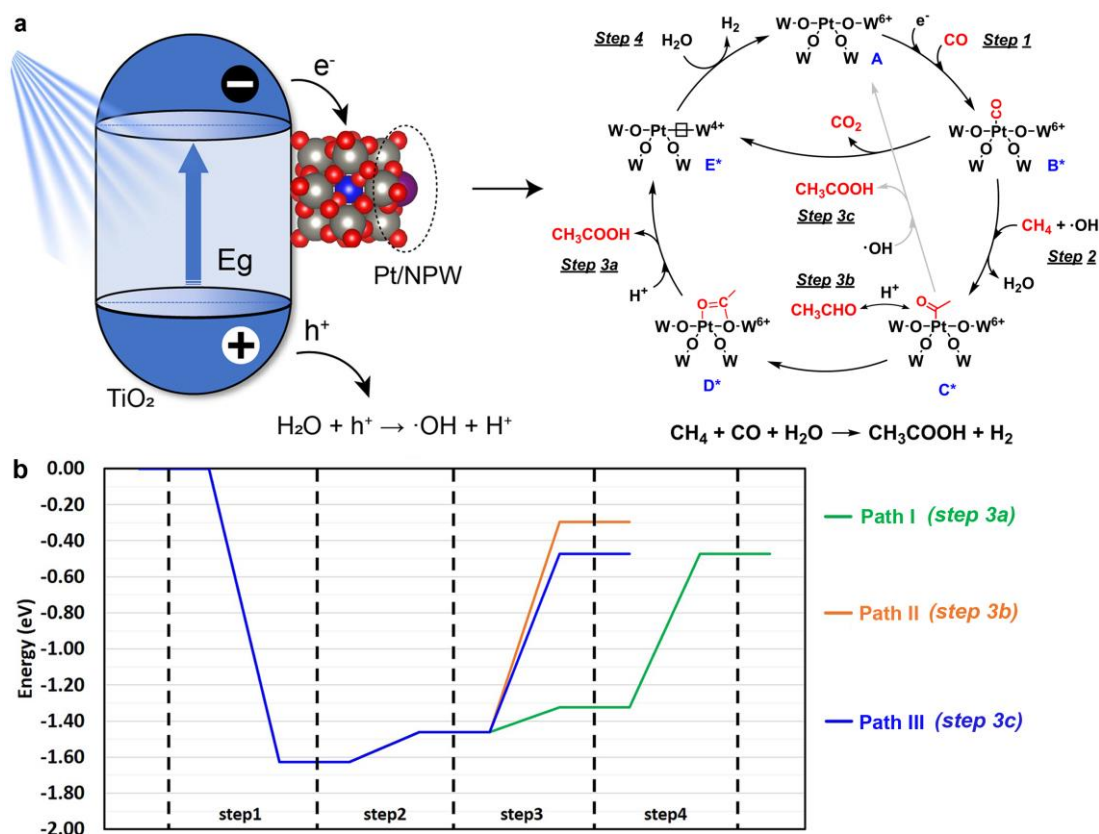
Figure 4. Reaction mechanism illustration. (a) Schematic illustration of the generation of photo-excited charge carriers and proposed mechanism of the photocatalytic AcOH generation process over a 4-fold oxygen coordinated Pt_1 site. Note

15

that from states B to E, the * marks the reduction state of NPW due to accepting photo-excited electrons from TiO_2. (b) The reaction energies (eV) corresponding to the elementary steps of gas phase reaction over Pt_1/NPW moiety for AcOH and acetaldehyde synthesis.

The proposed mechanism of AcOH synthesis from methane, CO and water is shown in **Figure 4a**. In agreement with the EPR results (**Figure S19**), the photo-excited electrons from TiO_2 upon UV irradiation, migrate to the surface of Pt/NPW clusters, while the holes remain on TiO_2 and react directly with H_2O to produce H protons (H^+) and ·OH. FTIR data suggest that CO adsorption takes place preferentially at Pt_1 sites (*step 1*). Methane is activated over Pt_1 sites by ·OH produced from water under irradiation and forms an acetyl group detected by FTIR which forms through C-C coupling with adsorbed CO (*step 2*).

Then, the acetyl group oxidizes into acetate and desorbs as AcOH (*step 3a*). Note that the AcOH desorption generates oxygen vacancies adjacent to Pt_1 sites and leads to the reduction of W^{6+} to W^{4+}. These oxygen vacancies are then filled by oxygen from H_2O molecules with the generation of H_2 and reoxidation of W^{4+} back to W^{6+} (*step 4*). Water dissociation over oxygen vacancies linked to single-atom Pt_1 species is well known in the literature and widely used in HER reaction for hydrogen generation.[55] The catalytic reaction involves lattice oxygen species of Pt/NPW dispersed over TiO_2 (Path I). Alternatively, AcOH also can be produced either via oxidation of acetaldehyde intermediate (*step 3b* in Path II) or the direct oxidation of the acetyl groups by ·OH (*step 3c* in Path III). We performed theoretical calculations to evaluate these possibilities. First, it appears that CO adsorption (*step 1*) is always highly exothermic (**Figure 4b**). At the same time, the coupling step to acetyl group is only slightly endothermic. As shown in **Figure 4b**, due to higher endothermicity, the formation of acetaldehyde through Path II is a less favorable route compared to that of AcOH. As for Path I and III, they exhibit similar energies to complete the reaction cycle. The most energy demanding step in the proposed MvK mechanism is the regeneration of the oxygen vacancies by H_2O (*step 4*). However, our in-situ XANES experiments showing

partial tungsten reduction (**Figure 3a**) and Bader charge analysis (**Figure S23**) give evidence in favor of the Mars van Krevelen type mechanism.

Conclusion

In summary, we demonstrated a new photocatalytic route, occurring at ambient temperature for direct conversion of CH_4, CO, and H_2O into AcOH over a composite, which is constituted by TiO_2 support and Pt_1 anchored NPW sub-nano clusters. The photocatalyst enables the selective and stable synthesis of AcOH, with a liquid-phase selectivity over 90 % and yielding the acetic acid solution with a concentration of 5.7 $mmol·L^{-1}$. Driven by the photo-generated charge carriers, CH_4 is activated by $·OH$ radicals and reacts with a CO molecule adsorbed over Pt_1 surface sites yielding an acetyl group. Further oxidation of acetyl group leads to acetic acid.

Supporting Information

Chemicals' information; experimental details; characterization methods; Gibbs free energy diagram; UV-Vis DRS spectra; UV-Vis absorption spectra; ^1H NMR spectra; performance of specific catalysts; performance comparison with literature; STEM and EDS-mapping images; mass spectrum; EPR spectra; standard curves for products' quantifications.

Acknowledgements

Competing Interests

The authors declare no competing interests.

References

1. Tang, P.; Zhu, Q.; Wu, Z.; Ma, D., Methane activation: the past and future. *Energy Environ. Sci.,* **2014,** *7* (8), 2580-2591.

2. Yu, X.; Zholobenko, V. L.; Moldovan, S.; Hu, D.; Wu, D.; Ordomsky, V. V.; Khodakov, A. Y., Stoichiometric methane conversion to ethane using photochemical looping at ambient temperature. *Nat. Energy* **2020,** *5* (7), 511-519.

3. Song, H.; Meng, X.; Wang, S.; Zhou, W.; Wang, X.; Kako, T.; Ye, J., Direct and Selective Photocatalytic Oxidation of CH_4 to Oxygenates with O_2 on Cocatalysts/ZnO at Room Temperature in Water. *J. Am. Chem. Soc.* **2019,** *141* (51), 20507-20515.

4. Yoneda, N.; Kusano, S.; Yasui, M.; Pujado, P.; Wilcher, S., Recent advances in processes and catalysts for the production of acetic acid. *Applied Catalysis A: General* **2001,** *221* (1), 253-265.

5. Yuan, Q.; Zhang, Q.; Wang, Y., Direct conversion of methane to methyl acetate with nitrous oxide and carbon monoxide over heterogeneous catalysts containing both rhodium and iron phosphate. *J. Catal.* **2005,** *233* (1), 221-233.

6. Periana, R. A.; Mironov, O.; Taube, D.; Bhalla, G.; Jones, C., Catalytic, Oxidative Condensation of CH_4 to CH_3COOH in One Step via CH Activation. *Science* **2003,** *301* (5634), 814-818.

7. Zerella, M.; Kahros, A.; Bell, A. T., Methane oxidation to acetic acid catalyzed by Pd^{2+} cations in the presence of oxygen. *J. Catal.* **2006,** *237* (1), 111-117.

8. Asadullah, M.; Kitamura, T.; Fujiwara, Y., Calcium-Catalyzed Selective and Quantitative Transformation of CH_4 and CO into Acetic Acid. *Angew Chem Int Ed Engl* **2000,** *39* (14), 2475-2478.

9. Reis, P. M.; Silva, J. A. L.; Palavra, A. F.; Fraústo da Silva, J. J. R.; Kitamura, T.; Fujiwara, Y.; Pombeiro, A. J. L., Single-Pot Conversion of Methane into Acetic Acid in the Absence of CO and with Vanadium Catalysts Such as Amavadine. *Angew Chem Int Ed Engl* **2003,** *42* (7), 821-823.

10. Lin, M.; Sen, A., Direct catalytic conversion of methane to acetic acid in an aqueous medium. *Nature* **1994,** *368* (6472), 613-615.

11. Lin, M.; Hogan, T. E.; Sen, A., Catalytic Carbon−Carbon and Carbon−Hydrogen Bond Cleavage in Lower Alkanes. Low-Temperature Hydroxylations and Hydroxycarbonylations with Dioxygen as the Oxidant. *J. Am. Chem. Soc.* **1996,** *118* (19), 4574-4580.

12. Shan, J.; Li, M.; Allard, L. F.; Lee, S.; Flytzani-Stephanopoulos, M., Mild oxidation of methane to methanol or acetic acid on supported isolated rhodium catalysts. *Nature* **2017,** *551* (7682), 605-608.

13. Tang, Y.; Li, Y.; Fung, V.; Jiang, D.-e.; Huang, W.; Zhang, S.; Iwasawa, Y.; Sakata, T.; Nguyen, L.; Zhang, X.; Frenkel, A. I.; Tao, F., Single rhodium atoms anchored in micropores for efficient transformation of methane under mild conditions. *Nat. Commun.* **2018,** *9* (1), 1231.

14. Lin, L.; Zhou, W.; Gao, R.; Yao, S.; Zhang, X.; Xu, W.; Zheng, S.; Jiang, Z.; Yu, Q.; Li, Y.-W.; Shi, C.; Wen, X.-D.; Ma, D., Low-temperature hydrogen production from water and methanol using Pt/α-MoC catalysts. *Nature* **2017,** *544* (7648), 80-83.

15. Sushkevich, V. L.; Palagin, D.; Ranocchiari, M.; van Bokhoven, J. A., Selective anaerobic oxidation of methane enables direct synthesis of methanol. *Science* **2017,** *356* (6337), 523-527.

16. Liu, Z.; Huang, E.; Orozco, I.; Liao, W.; Palomino Robert, M.; Rui, N.; Duchoň, T.; Nemšák, S.; Grinter David, C.; Mahapatra, M.; Liu, P.; Rodriguez José, A.; Senanayake Sanjaya, D., Water-promoted interfacial pathways in methane oxidation to methanol on a CeO_2-Cu_2O catalyst. *Science* **2020,** *368* (6490), 513-517.

17. Dong, C.; Lian, C.; Hu, S.; Deng, Z.; Gong, J.; Li, M.; Liu, H.; Xing, M.; Zhang, J., Size-dependent activity and selectivity of carbon dioxide photocatalytic reduction over platinum nanoparticles. *Nat. Commun.* **2018,** *9* (1), 1252.

18. Yu, X.; De Waele, V.; Löfberg, A.; Ordomsky, V.; Khodakov, A. Y., Selective photocatalytic conversion of methane into carbon monoxide over zinc-heteropolyacid-titania nanocomposites. *Nat. Commun.* **2019,** *10* (1), 700.

19. Wu, X.; Luo, N.; Xie, S.; Zhang, H.; Zhang, Q.; Wang, F.; Wang, Y., Photocatalytic transformations of lignocellulosic biomass into chemicals. *Chem. Soc. Rev.* **2020,** *49* (17), 6198-6223.

20. Song, S.; Song, H.; Li, L.; Wang, S.; Chu, W.; Peng, K.; Meng, X.; Wang, Q.; Deng, B.; Liu, Q.; Wang, Z.; Weng, Y.; Hu, H.; Lin, H.; Kako, T.; Ye, J., A selective Au-ZnO/TiO$_2$ hybrid photocatalyst for oxidative coupling of methane to ethane with dioxygen. *Nat. Catal.* **2021,** *4* (12), 1032-1042.

21. Li, X.; Wang, C.; Tang, J., Methane transformation by photocatalysis. *Nat. Rev. Mater.* **2022,** *7,* 617-632.

22. Chen, S.; Takata, T.; Domen, K., Particulate photocatalysts for overall water splitting. *Nat. Rev. Mater.* **2017,** *2* (10), 17050.

23. Wu, S.; Tan, X.; Lei, J.; Chen, H.; Wang, L.; Zhang, J., Ga-Doped and Pt-Loaded Porous TiO$_2$–SiO$_2$ for Photocatalytic Nonoxidative Coupling of Methane. *J. Am. Chem. Soc.* **2019,** *141* (16), 6592-6600.

24. Song, H.; Meng, X.; Wang, Z.-j.; Liu, H.; Ye, J., Solar-Energy-Mediated Methane Conversion. *Joule* **2019,** *3* (7), 1606-1636.

25. Hu, D.; Ordomsky, V. V.; Khodakov, A. Y., Major routes in the photocatalytic methane conversion into chemicals and fuels under mild conditions. *Applied Catalysis B: Environmental* **2021,** *286,* 119913.

26. Chen, Z.; Wu, S.; Ma, J.; Mine, S.; Toyao, T.; Matsuoka, M.; Wang, L.; Zhang, J., Non-oxidative Coupling of Methane: N-type Doping of Niobium Single Atoms in TiO$_2$–SiO$_2$ Induces Electron Localization. *Angew Chem Int Ed Engl* **2021,** *60* (21), 11901-11909.

27. Jiang, W.; Low, J.; Mao, K.; Duan, D.; Chen, S.; Liu, W.; Pao, C.-W.; Ma, J.; Sang, S.; Shu, C.; Zhan, X.; Qi, Z.; Zhang, H.; Liu, Z.; Wu, X.; Long, R.; Song, L.; Xiong, Y., Pd-Modified ZnO–Au Enabling Alkoxy Intermediates Formation and Dehydrogenation for Photocatalytic Conversion of Methane to Ethylene. *J. Am. Chem. Soc.* **2021,** *143* (1), 269-278.

28. Pope, M. T., Introduction to Polyoxometalate Chemistry. In *Polyoxometalate Molecular Science*, Borrás-Almenar, J. J.; Coronado, E.; Müller, A.; Pope, M., Eds. Springer Netherlands: Dordrecht, 2003; pp 3-31.

29. Sun, M.; Abou-Hamad, E.; Rossini, A. J.; Zhang, J.; Lesage, A.; Zhu, H.; Pelletier, J.; Emsley, L.; Caps, V.; Basset, J.-M., Methane Reacts with Heteropolyacids Chemisorbed on Silica to Produce Acetic Acid under Soft Conditions. *J. Am. Chem. Soc.* **2013,** *135* (2), 804-810.

30. Luo, L.; Gong, Z.; Xu, Y.; Ma, J.; Liu, H.; Xing, J.; Tang, J., Binary Au–Cu Reaction Sites Decorated ZnO for Selective Methane Oxidation to C1 Oxygenates with Nearly 100% Selectivity at Room Temperature. *J. Am. Chem. Soc.* **2021,** *144,* 740-750.

31. Li, X.; Xie, J.; Rao, H.; Wang, C.; Tang, J., Platinum-and CuO$_x$-Decorated TiO$_2$ Photocatalyst for Oxidative Coupling of Methane to C$_2$ Hydrocarbons in a Flow Reactor. *Angewandte Chemie* **2020,** *132* (44), 19870-19875.

32. Ishimaru, M.; Amano, F.; Akamoto, C.; Yamazoe, S., Methane coupling and hydrogen evolution induced by palladium-loaded gallium oxide photocatalysts in the presence of water vapor. *Journal of Catalysis* **2021,** *397,* 192-200.

33. Zhang, W.; Fu, C.; Low, J.; Duan, D.; Ma, J.; Jiang, W.; Chen, Y.; Liu, H.; Qi, Z.; Long, R.; Yao, Y.; Li, X.; Zhang, H.; Liu, Z.; Yang, J.; Zou, Z.; Xiong, Y., High-performance photocatalytic nonoxidative conversion of methane to ethane and hydrogen by heteroatoms-engineered TiO$_2$. *Nature Communications* **2022,** *13* (1), 2806.

34.   Huang, W.; Sun, W. Z.; Li, F., Efficient synthesis of ethanol and acetic acid from methane and carbon dioxide with a continuous, stepwise reactor. *AIChE Journal* **2010,** *56* (5), 1279-1284.

35.   Qi, G.; Davies, T. E.; Nasrallah, A.; Sainna, M. A.; Howe, A. G. R.; Lewis, R. J.; Quesne, M.; Catlow, C. R. A.; Willock, D. J.; He, Q.; Bethell, D.; Howard, M. J.; Murrer, B. A.; Harrison, B.; Kiely, C. J.; Zhao, X.; Deng, F.; Xu, J.; Hutchings, G. J., Au-ZSM-5 catalyses the selective oxidation of CH_4 to CH_3OH and CH_3COOH using O_2. *Nat. Catal.* **2022,** *5*, 45-54.

36.   Wu, B.; Lin, T.; Lu, Z.; Yu, X.; Huang, M.; Yang, R.; Wang, C.; Tian, C.; Li, J.; Sun, Y.; Zhong, L., Fe binuclear sites convert methane to acetic acid with ultrahigh selectivity. *Chem* **2022,** *8*, 1658-1672.

37.   Zhang, B.; Asakura, H.; Yan, N., Atomically Dispersed Rhodium on Self-Assembled Phosphotungstic Acid: Structural Features and Catalytic CO Oxidation Properties. *Ind. Eng. Chem. Res.* **2017,** *56* (13), 3578-3587.

38.   Zhang, B.; Sun, G.; Ding, S.; Asakura, H.; Zhang, J.; Sautet, P.; Yan, N., Atomically Dispersed Pt1–Polyoxometalate Catalysts: How Does Metal–Support Interaction Affect Stability and Hydrogenation Activity? *J. Am. Chem. Soc.* **2019,** *141* (20), 8185-8197.

39.   Hülsey, M. J.; Zhang, B.; Ma, Z.; Asakura, H.; Do, D. A.; Chen, W.; Tanaka, T.; Zhang, P.; Wu, Z.; Yan, N., In situ spectroscopy-guided engineering of rhodium single-atom catalysts for CO oxidation. *Nature Communications* **2019,** *10* (1), 1330.

40.   Qiao, B.; Wang, A.; Yang, X.; Allard, L. F.; Jiang, Z.; Cui, Y.; Liu, J.; Li, J.; Zhang, T., Single-atom catalysis of CO oxidation using Pt_1/FeO_x. *Nat. Chem.* **2011,** *3*, 634-641.

41.   DeRita, L.; Resasco, J.; Dai, S.; Boubnov, A.; Thang, H. V.; Hoffman, A. S.; Ro, I.; Graham, G. W.; Bare, S. R.; Pacchioni, G.; Pan, X.; Christopher, P., Structural evolution of atomically dispersed Pt catalysts dictates reactivity. *Nat. Mater.* **2019,** *18*, 746-751.

42.   DeRita, L.; Dai, S.; Lopez-Zepeda, K.; Pham, N.; Graham, G. W.; Pan, X.; Christopher, P., Catalyst Architecture for Stable Single Atom Dispersion Enables Site-Specific Spectroscopic and Reactivity Measurements of CO Adsorbed to Pt Atoms, Oxidized Pt Clusters, and Metallic Pt Clusters on TiO_2. *J. Am. Chem. Soc.* **2017,** *139* (40), 14150-14165.

43.   Therrien, A. J.; Hensley, A. J. R.; Marcinkowski, M. D.; Zhang, R.; Lucci, F. R.; Coughlin, B.; Schilling, A. C.; McEwen, J.-S.; Sykes, E. C. H., An atomic-scale view of single-site Pt catalysis for low-temperature CO oxidation. *Nat. Catal.* **2018,** *1* (3), 192-198.

44.   Zheng, Y.; Duan, Y.; Tang, H.; Li, C.; Li, J.; Zhu, C.; Liu, S., Experimental research on selective adsorption of gaseous mercury (II) over SiO2, TiO2 and γ-Al2O3. *Fuel* **2019,** *237*, 202-208.

45.   Xiao, J.; Mao, D.; Guo, X.; Yu, J., Effect of TiO2, ZrO2, and TiO2–ZrO2 on the performance of CuO–ZnO catalyst for CO2 hydrogenation to methanol. *Applied Surface Science* **2015,** *338*, 146-153.

46.   Yamazoe, S.; Hitomi, Y.; Shishido, T.; Tanaka, T., XAFS Study of Tungsten L_1- and L_3-Edges: Structural Analysis of WO3 Species Loaded on TiO2 as a Catalyst for Photo-oxidation of NH3. *J. Phys. Chem. C* **2008,** *112* (17), 6869-6879.

47.   Jayarathne, U.; Chandrasekaran, P.; Greene, A. F.; Mague, J. T.; DeBeer, S.; Lancaster, K. M.; Sproules, S.; Donahue, J. P., X-ray Absorption Spectroscopy Systematics at the Tungsten L-Edge. *Inorg. Chem.* **2014,** *53* (16), 8230-8241.

48.   Pazé, C.; Bordiga, S.; Zecchina, A., H_2O Interaction with Solid $H_3PW_{12}O_{40}$: An IR Study. *Langmuir* **2000,** *16* (21), 8139-8144.

49.   Demri, D.; Hindermann, J.-P.; Diagne, C.; Kiennemann, A., Formation of C_2 oxygenates on rhodium-containing catalysts during $CO + H_2$ reactions. FTIR study of acetaldehyde adsorption. *J. Chem. Soc. Faraday Trans.* **1994,** *90* (3), 501-506.

50. Rachmady, W.; Vannice, M. A., Acetic Acid Reduction by H_2 over Supported Pt Catalysts: A DRIFTS and TPD/TPR Study. *J. Catal.* **2002,** *207* (2), 317-330.

51. Pei, Z. F.; Ponec, V., On the intermediates of the acetic acid reactions on oxides: an IR study. *Appl. Surf. Sci.* **1996,** *103* (2), 171-182.

52. Dimitrijevic, N. M.; Vijayan, B. K.; Poluektov, O. G.; Rajh, T.; Gray, K. A.; He, H.; Zapol, P., Role of Water and Carbonates in Photocatalytic Transformation of CO_2 to CH_4 on Titania. *J. Am. Chem. Soc.* **2011,** *133* (11), 3964-3971.

53. Amthor, S.; Knoll, S.; Heiland, M.; Zedler, L.; Li, C.; Nauroozi, D.; Tobaschus, W.; Mengele, A. K.; Anjass, M.; Schubert, U. S.; Dietzek-Ivanšić, B.; Rau, S.; Streb, C., A photosensitizer–polyoxometalate dyad that enables the decoupling of light and dark reactions for delayed on-demand solar hydrogen production. *Nat. Chem.* **2022,** *14*, 321-327.

54. Meng, X.; Cui, X.; Rajan, N. P.; Yu, L.; Deng, D.; Bao, X., Direct Methane Conversion under Mild Condition by Thermo-, Electro-, or Photocatalysis. *Chem* **2019,** *5* (9), 2296-2325.

55. Ye, S.; Xiong, W.; Liao, P.; Zheng, L.; Ren, X.; He, C.; Zhang, Q.; Liu, J., Removing the barrier to water dissociation on single-atom Pt sites decorated with a CoP mesoporous nanosheet array to achieve improved hydrogen evolution. *Journal of Materials Chemistry A* **2020,** *8* (22), 11246-11254.

TOC Graphic